ARTICLE

Acoustic modes of a spherical thin-walled tank for liquid propellant mass gauging: Theory and experiment

Cyrill B. Muratov,[1,a)] Joseph Rogers,[2] and Michael Khasin[3,b)]

[1]*Department of Mathematical Sciences, New Jersey Institute of Technology, Newark, New Jersey 07102, USA*

[2]*KBRwyle LLC, National Aeronautics and Space Administration Ames Research Center, Moffett Field, California 94035, USA*

[3]*National Aeronautics and Space Administration Ames Research Center, Moffett Field, California 94035, USA*

ABSTRACT:

Acoustic response of a thin-walled spherical flight tank filled with water is explored theoretically and experimentally as a testbed for an application of Weyl's law to the problem of mass-gauging propellants in zero-gravity in space. Weyl's law relates the mode counting function of a resonator to its volume and can be used to infer the volume of liquid in a tank from the tank's acoustic response. One of the challenges of applying Weyl's law to real tanks is to account for the boundary conditions which are neither Neumann nor Dirichlet. We show that the liquid modes in a thin-walled spherical tank correspond to the spectrum of a slightly larger spherical tank with infinitely compliant wall (Dirichlet boundary condition), where Weyl's law can be applied directly. The mass of the liquid enclosed by this "effective" tank's wall is found to equal the actual mass of the liquid plus the mass of the wall. This finding is generalized to thin-walled tanks and liquid configurations of arbitrary shapes and thus provides a calculable correction factor for the propellant mass inferred using Weyl's law with Dirichlet boundary conditions.
https://doi.org/10.1121/10.0016357

I. INTRODUCTION

Accurate assessment of the amount of available liquid propellant in a tank—propellant mass gauging—in zero or reduced gravity is a critical enabling technology for rocket propulsion and in-space propellant storage required in the next generation of space exploration missions.[1,2] Gauging the amount of available liquid in a tank in reduced gravity poses fundamental technical challenges due to a variable and unpredictable configuration of the liquid in the tank. For Earth's gravity and settled liquid conditions in general, a range of mass gauging techniques are available.[3–5] However, liquid mass gauging becomes a significant challenge under microgravity conditions where both the location and the shape of the gas-liquid interface are unknown (see Refs. 6–10 for some proposed approaches). These effects result from the dominance of surface tension and capillary forces in the absence of significant gravitational forces on the liquid.[5] In this regime, the shape of the gas-liquid interface is dictated almost exclusively by the container geometry and the liquid-container wettability. Furthermore, the mechanical equilibrium of the liquid may be close to neutral, and small time-dependent perturbations can slowly, but dramatically, change the observed liquid configuration over time.[5]

Spectral mass gauging (SMG) is a promising non-invasive acoustic technology for mass-gauging, proposed in

Ref. 9. SMG is based on an application of Weyl's law[11] to the problem of mass-gauging. Generally, Weyl's law expresses the asymptotic behavior of the eigenvalues counting function of the Laplacian operator in a bounded domain with suitable boundary conditions.[12] The asymptotic expression (see Sec. II) relates the counting function to the volume of the domain. The SMG method relies on the ability to actuate the first few thousands of vibration eigenmodes of the liquid-filled tank by tapping on the tank's wall from the outside and to count the corresponding eigenfrequencies.[9] By extracting the leading order high-frequency asymptotic behavior of the measured counting function one can in principle recover the liquid volume with arbitrary precision from the known parameters of the liquid independently of the shape of the liquid body in the tank or the shape of the tank.

In application to the vibration spectrum of a chamber Weyl's law is valid for two extreme kinds of boundary conditions: (i) pressure release boundary condition corresponding to an infinitely compliant wall of the chamber (Dirichlet boundary condition) or (ii) an infinitely rigid wall (Neumann boundary condition). Weyl's law for vibration spectra corresponding to Neumann boundary condition were in the focus of the early studies of the distribution of eigentones in rectangular chambers in application to room acoustic.[13–15] Recently Weyl's law was applied at NIST in metrological studies of gas-filled pressure vessels,[16] where the rigid wall boundary condition was expected to be accurate.

The acoustic spectrum of a real liquid-filled tank is different from these two extreme cases due to the complicated

a)Also at: Dipartimento di Matematica, Università di Pisa, Largo B. Pontecorvo 5, Pisa 56127, Italy.
b)Electronic mail: michael.khasin@nasa.gov

interaction of the liquid inside the tank with the elastic solid walls enclosing it. The goal of the present work is to explore this interaction both theoretically and experimentally in the context of SMG. In Sec. II, we briefly review Weyl's law and formulate a model of a thin-walled spherical tank. Section III is dedicated to calculating the tank's vibration spectrum. We note that vibration spectrum of a gas-filled thick-walled pressure tank was calculated in Ref. 17 for a spherical geometry and in Ref. 18 for a quasi-spherical tank. In Ref. 19 the model developed in Ref. 17 was applied to a liquid-filled thick-walled spherical pressure vessel. Here, we focus on the essentially opposite limit of a thin-walled liquid filled tank which is relevant for applications to propellant tanks in space. In the obtained spectrum, we distinguish between the shell modes, which are localized in the vicinity of the wall, and the liquid modes, which are delocalized throughout the bulk of the liquid. We find that for sufficiently low frequencies (the soft wall regime) the liquid modes can be represented as a perturbation of the spectrum of a sphere with Dirichlet boundary conditions, while for sufficiently high frequencies (the rigid wall regime) they can be represented as a perturbation of the spectrum of a sphere with Neumann boundary conditions and quantify these perturbations. Section IV presents experimental results for testing the acoustic spectrum of a thin-walled spherical titanium flight tank filled with water. The agreement of the measured spectra to the analytical predictions of Sec. III is found to be excellent both for the shell modes and the liquid modes.

Our main theoretical finding in Sec. III in the context of SMG is that in the first order of the small parameter, which is essentially the ratio of the wall mass to the liquid mass in the tank, the spectrum in the soft wall regime is equivalent to that of a spherical tank with a perfectly compliant wall (Dirichlet boundary condition), but having a larger radius. Accordingly, Weyl's law can be applied to accurately infer the volume of the tank by correcting for this effective radius increase. Specifically, we show in Sec. V that the mass of the liquid enclosed in the larger "effective" tank simply equals the mass of the liquid in the original tank plus the added mass of the tank wall. Importantly, this result remains true for partially filled thin-walled tanks of arbitrary shapes (see Appendix C), namely, the added mass inferred from the application of Weyl's law to a thin-walled propellant tank *is equal to the mass of the tank wall in contact with the liquid* to the first order in the wall thickness. The utility of this result is significant for in-space applications, since in zero gravity the propellant configuration in a partially filled tank is not known, but the propellant wets the tank walls completely and, therefore, is in contact with the entire wall surface. In this situation, the tank-wall correction is independent of the unknown propellant configuration and equal to the total mass of the tank wall, which is generally known and can be taken into account for the propellant mass inference. Section VI summarizes our conclusions.

II. LIQUID VIBRATIONS WITHIN A SPHERICAL ELASTIC SHELL

The idea behind the SMG method relies on the asymptotic behavior of the eigenvalue counting function of the Laplacian operator in a bounded domain with suitable boundary conditions (Weyl's law), which can be expressed in terms of the counting function $N(f)$ of the eigenfrequencies associated with the wave equation satisfied by the pressure p in the liquid:

$$\partial_t^2 p = c_L^2 \Delta p \quad \text{in} \quad \Omega_L, \tag{1}$$

where Ω_L is the liquid-filled domain, c_L is the speed of sound in the liquid phase and Δ denotes the three-dimensional Laplacian. The eigenfrequency counting function is defined as

$$N(f) = \sum_{k=1}^{\infty} \theta(f - f_k), \tag{2}$$

where $\theta(t)$ is the Heaviside step function and f_k are the eigenfrequencies that satisfy

$$-c_L^2 \Delta \psi_k = (2\pi f_k)^2 \psi_k \quad \text{in} \quad \Omega_L, \tag{3}$$

with the appropriate boundary conditions. The eigenfunction ψ_k is the normal mode associated with the kth eigenfrequency. Weyl's Law[11,12] states that the counting function $N(f)$ has the following asymptotic expansion:

$$N(f) = \frac{4\pi V f^3}{3c_L^3} + \frac{\pi A f^2}{4c_L^2} + o(f^2), \quad f \to \infty, \tag{4}$$

where V is the volume of the space occupied by the liquid. In the case of pressure release boundary condition corresponding to the liquid-gas interfaces and a compliant tank wall the value of A is equal to the negative total surface area of $\partial\Omega_L$; for the rigid wall and a full tank the value of A equals the total surface area of $\partial\Omega_L$. By extracting the leading order asymptotic behavior of the measured counting function $N(f)$ as $f \to \infty$, one can, therefore, in principle recover the liquid volume V with arbitrary precision from the known parameters of the liquid independently of the shape of Ω_L.

In this section we derive a model describing the vibrational modes of a liquid-filled spherical tank motivated by the specifications of the test tank used at NASA Ames Research Center to validate the SMG technique on the ground. The latter consists of a titanium spherical shell of inner radius $R = 37.6$ cm and wall thickness $d_w = 1.27$ mm. The material parameters of pure titanium are mass density $\rho_w = 4506$ kg/m^3, Young modulus $E = 1.16 \times 10^{11}$ Pa, and Poisson ratio $\sigma = 0.32$. The working liquid is water, whose parameters are mass density $\rho_L = 1000$ kg/m^3 and sound speed $c_L = 1450$ m/s. Our model neglects the irreversible dissipation mechanisms or acoustic radiation and treats the tank wall as an infinitesimally thin elastic shell.

J. Acoust. Soc. Am. **152** (6), December 2022

Muratov *et al.* 3261

We begin by stating the acoustic equation for the liquid.[20] Let $B_R \subset \mathbb{R}^3$ be a ball of radius R centered at the origin that is enclosed by an elastic shell. Introducing the velocity potential φ, we can write

$$\partial_t^2 \varphi = c_L^2 \Delta \varphi \quad \text{in} \quad B_R. \tag{5}$$

Turning to the boundary conditions, on ∂B_R we introduce the displacement ζ of the shell in the direction of the outer normal to ∂B_R. Noting that the rate of displacement coincides with the normal liquid velocity, from the definition $\mathbf{v} = \nabla \varphi$ for the liquid velocity we obtain the kinematic condition

$$\partial_t \zeta = \partial_n \varphi \quad \text{on} \quad \partial B_R, \tag{6}$$

where ∂_n denotes the derivative in the direction of the outward normal to ∂B_R. We also need to match the pressure jump due to shell elasticity on both sides of ∂B_R, assuming zero pressure on the outer surface of the shell. Again, recalling that the acoustic pressure in the liquid is given by $p = -\rho_L \partial_t \varphi$ and using the expression for the pressure difference across a thin elastic shell from Refs. 21 and 22 yields

$$\rho_w d_w \partial_t^2 \zeta = -\rho_L \partial_t \varphi - B \Delta_\perp^2 \zeta - R^{-1} \Delta_\perp \psi \quad \text{on} \quad \partial B_R, \tag{7}$$

where $\Delta_\perp$ is the Laplace-Beltrami operator on ∂B_R, ψ is the Airy stress function solving

$$\Delta_\perp^2 \psi = S R^{-1} \Delta_\perp \zeta \tag{8}$$

and

$$B = \frac{E d_w^3}{12(1 - \sigma^2)}, \quad S = E d_w \tag{9}$$

are the bending and stretching stiffnesses, respectively. Here, for simplicity we used the shallow shell approximation that should be appropriate for the high transverse wave number regime we are interested in.

Eliminating the Airy stress ψ yields

$$\rho_w d_w \partial_t^2 \zeta = -\rho_L \partial_t \varphi - B \Delta_\perp^2 \zeta - S R^{-2} \zeta \quad \text{on} \quad \partial B_R, \tag{10}$$

which together with Eq. (6) specifies the boundary conditions for Eq. (5). Dimensional analysis of Eq. (10) suggests that bending and stretching terms dominate depending on the scale ℓ of variation of ζ along ∂B_R. For $\ell \lesssim \ell_{wb}$, where $\ell_{wb} = (d_w R)^{1/2} = 2.2$ cm, the bending term dominates, while for $\ell \gtrsim \ell_{wb}$ the stretching term dominates. Also, the inertia of the wall dominates when $\rho_w d_w \gtrsim \rho_L \ell$, i.e., when $\ell \lesssim \ell_{wi} = \rho_w d_w / \rho_L = 6\,\text{mm}$.

III. HIGH FREQUENCY NORMAL MODES

In this section we use Eqs. (5), (6), and (10) to identify the normal acoustic modes dominated by liquid and shell vibrations. This is achieved by passing to time harmonic equations with

$$\varphi_L(x, t) = a(r) e^{-i\omega t} Y_{nm}(\theta, \phi),$$
$$\zeta(x, t) = b e^{-i\omega t} Y_{nm}(\theta, \phi), \tag{11}$$

where (r, θ, ϕ) are spherical coordinates and Y_{nm} are spherical harmonics with $n = 0, 1, 2, \ldots$ and $|m| \leq n$. Substituting this expression for φ into Eq. (5) yields $a(r) = A j_n(\omega r / c_L)$, where j_n is the spherical Bessel function of the first kind,[23] and we took into account boundedness of the solution at the origin.

Turning to the boundary condition in Eq. (6), we find that

$$c_L b = i A j_n'(\omega R / c_L), \tag{12}$$

and we note the expression for the derivative of $j_n(z)$,[23]

$$j_n'(z) = \frac{n j_n(z)}{z} - j_{n+1}(z). \tag{13}$$

Using the second boundary condition in Eq. (7), we obtain the characteristic equation determining the eigenfrequency ω,

$$c_L \rho_L \omega \left(\frac{c_L n}{\omega R} - \frac{j_{n+1}(\omega R / c_L)}{j_n(\omega R / c_L)} \right)^{-1}$$
$$= \frac{B n^2 (n+1)^2}{R^4} + \frac{S}{R^2} - \rho_w d_w \omega^2. \tag{14}$$

Introducing the dimensionless frequency parameter $\lambda = \omega R / c_L$, this equation can be written as

$$\varepsilon + \left(n - \frac{\lambda j_{n+1}(\lambda)}{j_n(\lambda)} \right)^{-1} = \frac{\kappa_n}{\lambda^2}, \tag{15}$$

where

$$\varepsilon = \rho_w d_w / (\rho_L R), \quad \kappa_n = \frac{E d_w}{\rho_L c_L^2 R} \left(1 + \frac{n^2 (n+1)^2 d_w^2}{12(1 - \sigma^2) R^2} \right) \tag{16}$$

are two dimensionless parameters characterizing the inertia and the bending stiffness of the tank wall for a given mode, respectively. For our tank filled with water we have $\varepsilon \approx 0.015$ and $\kappa_0 \approx 0.18$.

We denote the roots of Eq. (15) by $\lambda_{n,k}$, where the radial wave number $k = 0, 1, 2, \ldots$, enumerates the distinct modes associated with the azimuthal wave number n in the ascending order. Analysis of Eq. (15) in Appendix A shows the following property of the spectrum: $0 < \lambda_{n,0} < a_{n,1}'$ and $a_{n,k}' < \lambda_{n,k} < a_{n,k+1}'$ for $k \geq 1$, where $a_{n,k}'$ denotes the kth zero of $j_n'(z)$, corresponding to the spectrum of a spherical tank with infinitely rigid walls (Neumann boundary conditions). Figure 1 illustrates this property by showing locations of the roots $\lambda_{n,k}$ and zeros $a_{n,k}'$ for $n = 10$, for parameters $\varepsilon \approx 0.015$ and $\kappa_0 \approx 0.18$ corresponding to the water-filled tank.

We note one immediate important consequence of the proved structure of the spectrum: since the spectrum corresponding to the Neumann boundary conditions satisfies
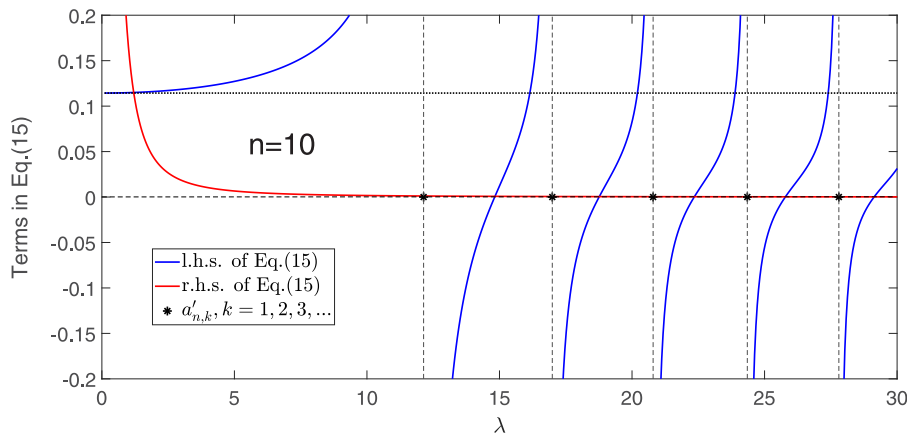
FIG. 1. (Color online) Plots of the left-hand side (blue) and the right-hand side (red) of Eq. (15) for $n = 10$, $\varepsilon \approx 0.015$ and $\kappa_0 \approx 0.18$, corresponding to the water-filled tank. Their intersection shows locations of the roots $\lambda_{n,k}$ of Eq. (15). Stars denote the locations of $a'_{n,k}$. It can be seen that $0 < \lambda_{n,0} < a'_{n,1}$ and $a'_{n,k} < \lambda_{n,k} < a'_{n,k+1}$ for $k \geq 1$, in agreement with the analysis in Appendix A. Black dotted line corresponds to $\varepsilon + 1/n$ on the vertical axis.

Weyl's law [see Eq. (4)], the spectrum $\lambda_{n,k}$ of a thin-walled tank will also satisfy Weyl's law to the leading $O(f^3)$ order in frequency as $f \to \infty$. Note that in Sec. V we show how Weyl's law may be applied to the spectrum of a thin-walled water-filled tank to the sub-leading $O(f^2)$ order.

The structure of the spectrum simplifies under the assumption $\lambda \ll n$, for which a closed form asymptotic expression may be derived. Using Eq. (9.1.73) in Ref. 23, we find that $j_{n+1}(z)/j_n(z) \simeq z/(2n+3)$ for $z \ll n$. Therefore, solving Eq. (15) we obtain a unique mode

$$\lambda_{n,0} \simeq \sqrt{\frac{n\kappa_n}{\varepsilon n + 1}}, \qquad \lambda_{n,0} \ll n, \tag{17}$$

where we noted that the obtained solution lies below $a'_{n,1} \simeq n + 1/2$ by Eq. (10.1.59) of Ref. 23 and is, therefore, the smallest for a given n. This expression is valid as long as $\kappa_n \ll n(\varepsilon n + 1)$ in order to be consistent and breaks down when $\kappa_n = n(\varepsilon n + 1)$. It is not difficult to see that the latter equation has two positive roots $n = n_c^{\pm}$ for all sufficiently small d_w/R, and Eq. (17) is thus valid when $n_c^- \ll n \ll n_c^+$ in this regime. Asymptotically, as $d_w/R \to 0$, i.e., in the limit of a thin-walled tank, we have $n_c^+ \simeq CR/d_w$, where the dimensionless constant C only depends on the material parameters and solves a cubic equation. Similarly, we have $n_c^- \simeq (E/\rho_L c_L^2)(d_w/R)$ as $d_w/R \to 0$. For the material parameters of a water-filled titanium tank we find $n_c^+ \simeq R/d_w$ and $n_c^- \simeq 55 d_w/R$. Therefore, in our water-filled

tank Eq. (17) is valid when $0.2 \ll n \ll 300$, i.e., Eq. (17) is valid for all $n \ll n_c^+$.

The structure of the spectrum simplifies in the range of validity of Eq. (17), where the spectrum can be separated into two groups. The first is a branch given by the roots $\lambda_{n,0}$, corresponding to the modes localized in the vicinity of the wall. The localization length l_n of these modes in the radial direction from the wall can be estimated as $l_n^{-1} \sim (d/dr)\log(j_n(\lambda_{n,0}r/R))|_{r=R}$. Using approximation $j'_n(z) \approx n j_n(z)/z$ valid for $z \ll n$, we find $l_n \approx R/n$. Those are evanescent modes, which will be termed *shell modes*, as their presence is due to the elasticity of the shell. As follows from Eq. (17), we have $\lambda_{n,0} \to 0$ as $d_w/R \to 0$. Figure 2 shows the numerical solution of Eq. (15) for the shell modes $\lambda_{n,0}$ in the water-filled tank. The expression in Eq. (17) is shown to agree well with the exact solution for $n \lesssim n_c^+ \approx 320$. For $n \gg n_c^+$, $\lambda_{n,0}$ is seen to asymptotically approach $a'_{n,1}$.

The second group of solutions of Eq. (15) corresponds to $\lambda_{n,k}$ for $k > 0$, which will be termed *liquid modes* for the reasons which will become clear below.

In Appendix B, we use perturbation theory to show that the κ_n/λ^2 term in Eq. (15) may be neglected in the calculation of $\lambda_{n,k}$ for $k > 0$, provided $\kappa_n \ll (1-\varepsilon)\sqrt{n(n+1)}$. For the parameters of the water-filled tank, we find that the latter condition is satisfied for $n \ll n_c^+$. It means that the elasticity terms do not affect the boundary conditions when $n \ll n_c^+$, and the liquid modes are effectively governed by the inertia
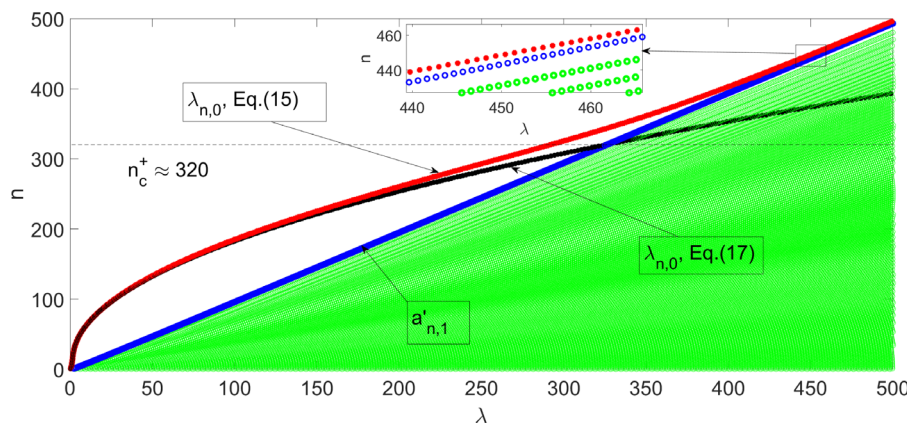

FIG. 2. (Color online) Numerical solution of Eq. (15) for the shell modes frequencies $\lambda_{n,0}$ (red) in the water-filled tank. Green circles (magnified in the insert) correspond to $\lambda_{n,k}$ with $k > 0$. Solution of approximate Eq. (17) (black) is shown to correspond well to the exact solution for $n \lesssim n_c \approx 320$, as found from solving $\kappa_{n_c^+} = n_c^+(\varepsilon n_c^+ + 1)$ numerically. For $n \gg n_c^+$, $\lambda_{n,0}$ is seen to asymptotically approach $a'_{n,1}$ (blue).

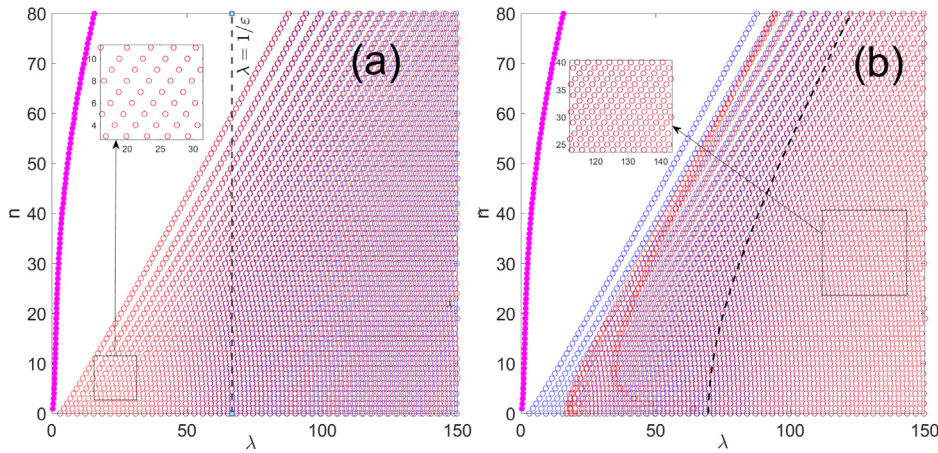J. Acoust. Soc. Am. **152** (6), December 2022

Muratov et al.   3263

FIG. 3. (Color online) Numerical solution of Eq. (15) for the shell modes $\lambda_{n,0}$ (magenta) and liquid modes $\lambda_{n,k}$ (blue circles) in the water-filled tank. Solutions of approximate Eqs. (19) (a) and (20) (b) are shown by red circles. They correspond very well to the exact solution in their regions of validity demarcated by the dashed lines $\lambda_{n,k} = \varepsilon^{-1}$ (a) and $\lambda_{n,k} = (2\varepsilon)^{-1} + \sqrt{(2\varepsilon)^{-2} + n(n+1)}$ (b).

of the wall in the water-filled tank. As a result, the following approximation for Eq. (15) holds:

$$\varepsilon + \left(n - \frac{\lambda j_{n+1}(\lambda)}{j_n(\lambda)} \right)^{-1} \simeq 0. \tag{18}$$

Two limits of Eq. (18) are considered next: the soft wall limit for $\lambda \ll \varepsilon^{-1}$ and the rigid wall limit for $\lambda \gg \varepsilon^{-1}$. In Appendix B, we show that in the soft wall limit we have

$$\lambda_{n,k} \simeq a_{n,k}(1 - \varepsilon), \quad \lambda_{n,k} \ll \varepsilon^{-1}. \tag{19}$$

We note that the condition $\lambda_{n,k} \ll \varepsilon^{-1}$ has a clear physical meaning: the soft wall approximation is valid for sufficiently long wave-lengths, such that the mass of the liquid per unit area of the wall in a layer of one wavelength width is much larger than the mass of the wall per unit area. In contrast to the shell modes, $\lambda_{n,k}$ for $k > 0$ have a non-singular limit as the wall becomes infinitely thin: $\lambda_{n,k} \to a_{n,k}$ as $\varepsilon, \kappa_n \sim d_w/R \to 0$. Since $a_{n,k}$ give the spectrum of a liquid sphere (with Dirichlet boundary conditions), this property justifies using the term *liquid modes* for $\lambda_{n,k}$ with $k > 0$. It is important to note that in the first order in ε the soft wall approximation in Eq. (19) is equivalent to the spectrum obtained for the Dirichlet boundary conditions for the sphere of radius $R' = R/(1 - \varepsilon)$. This follows immediately from the expression for the spectrum $f_{n,k} = \lambda_{n,k} c_L/(2\pi R) = a_{n,k}(1 - \varepsilon)c_L/(2\pi R)$, corresponding to Eq. (19). The implications of this observation will be explored in Sec. V.

In the limit of a rigid wall, the derivation in Appendix B yields

$$\lambda_{n,k} \simeq a'_{n,k} + \frac{1}{\varepsilon a'_{n,k} \left(1 - \dfrac{n(n+1)}{\left(a'_{n,k} \right)^2} \right)},$$

$$\lambda_{n,k} \gg (2\varepsilon)^{-1} + \sqrt{(2\varepsilon)^{-2} + n(n+1)}. \tag{20}$$

Note that in contrast to the soft wall limit $\lambda_{n,k} \ll \varepsilon^{-1}$, where all the modes in the corresponding frequency range are approximated well by those with the Dirichlet boundary condition, the assumption $\lambda_{n,k} \gg \varepsilon^{-1}$ is no longer sufficient

and the rigid wall approximation breaks down for the modes where $\lambda_{n,k} \sim n$.

Figure 3 demonstrates the high accuracy of the approximations in Eqs. (19) and (20) in their corresponding regions of validity.

IV. MEASURING THE ACOUSTIC RESPONSE OF A SPHERICAL TANK

This section presents data on acoustic spectra of the spherical tank modeled above. The data were collected for the water-filled ("full") tank configuration. The spherical tank is mounted as shown in Fig. 4(a). The hardware used for the testing consisted of solenoid actuators and accelerometers. The solenoids were mounted in frames to allow easy attachment and relocation [Fig. 4(b)]. Varying the actuation voltage to the solenoid from 6 to 18 V allowed various strike forces to be applied. The accelerometers [Figs. 4(c), 4(d)] tested had a range of sensitivities from 100–1000 mV/g ($g = 9.8$ m/s^2). A National Instruments hardware interface to a PC running an in-house developed LABVIEW routine were used for data acquisition.

Acoustic response was actuated by a single ping by a solenoid actuator to the tank wall. The time-series was collected by the NI and imported to MATLAB where processing of the data were performed to attenuate the shell modes and
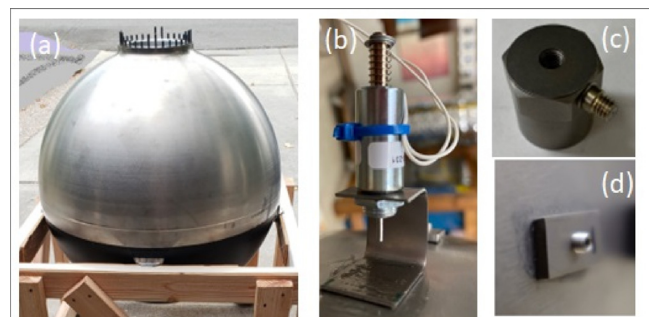

FIG. 4. (Color online) Hardware used for acoustic testing of the spherical tank: spherical titanium tank (a); solenoid actuator mounted on the tank wall via a metal frame epoxied to the wall (b), accelerometer (c), and accelerometer stud expoxied to the tank wall (d). A National Instruments hardware interface to a PC running an in-house developed LABVIEW routine were used for data collection.

3264   J. Acoust. Soc. Am. **152** (6), December 2022

Muratov *et al.*

compute the Fourier transform. Figure 5 shows the Fourier amplitude spectrum of the acoustic response of the water-filled tank to a single ping of an actuator. The red circles correspond to the numerical solution of Eq. (15) for the liquid modes. The magenta dots correspond to the theoretical prediction for the first 50 shell modes where they have the highest density, see Fig. 3. The shell modes at high wavenumbers n have been effectively eliminated from the spectra to facilitate liquid modes counting, using a pre-processing approach described in Ref. 24. This approach is based on the observation that damping rates of the shell modes are much higher than damping rates of the liquid modes in a given frequency interval due to the strong localization of the shell modes near the wall. The damping rate scale separation suggests a simple but efficient approach to eliminate the shell-mode contribution to the tank acoustic spectrum via an application of a time delay to the time-domain signal before transforming to the frequency domain. The time delay leads to an exponential suppression of the shell modes compared to the liquid modes due to damping. The correspondence of the experimental liquid-modes spectra to the theoretical predictions in Fig. 3 is excellent. The $(2n + 1)$-fold-degenerate liquid modes corresponding to a given (n, k) pair are seen to be split [subplot (c)], by an inevitable slight deviation of the tank geometry from the ideal spherical symmetry.

V. CONVERGENCE OF THE THEORETICAL MODE COUNTING FUNCTION TO WEYL'S LAW ASYMPTOTICS

In Sec. II we found that the crossover from the soft wall limit Eq. (19) to the rigid wall limit Eq. (20) occurs around $\lambda \sim \varepsilon^{-1}$. For the tested tank the corresponding frequency is

$f \sim c_L/(2\pi\varepsilon R) \approx 40\,\text{kHz}$. Accordingly, in the range of frequencies shown in Fig. 5 the soft wall approximation is valid. As noted in the end of Sec. III, the soft wall approximation is equivalent, in the first order in ε, to the spectrum obtained for the Dirichlet boundary condition for the sphere of radius $R' = R/(1 - \varepsilon)$. Therefore, fitting the resulting mode counting function $N(f)$ to the Weyl's law in Eq. (4) is expected to predict the volume of that effective sphere,

$$V' = \frac{4\pi R'^3}{3} = \frac{V}{(1 - \varepsilon)^3}. \tag{21}$$

An interesting interpretation of that result is given by considering the mass of the liquid inferred from Eq. (21),

$$M' = \frac{\rho_L V}{(1 - \varepsilon)^3} \approx \rho_L V(1 + 3\varepsilon) = M + M_w, \tag{22}$$

$$M_w = 4\pi R^2 \rho_w d_w.$$

It follows that fitting the mode counting function of the spherical tank in the range of validity of Eq. (19) predicts an effective mass of the liquid which is equal to the sum of the actual mass of the liquid M and the mass of the tank's wall M_w—the tank wall correction.

Figure 6(a) depicts the counting functions for both the spherical tank and the effective sphere. The correspondence is excellent in the range $f \lesssim 40$ kHz, as predicted. Figure 6(b) shows the corresponding volumes inferred from the counting functions using frequency-averaged Richardson extrapolation[25] to fit the counting functions to Weyl's law, Eq. (4). We see that a larger volume is predicted, given by Eq. (21). Figure 6(c) shows the error in the mass inference
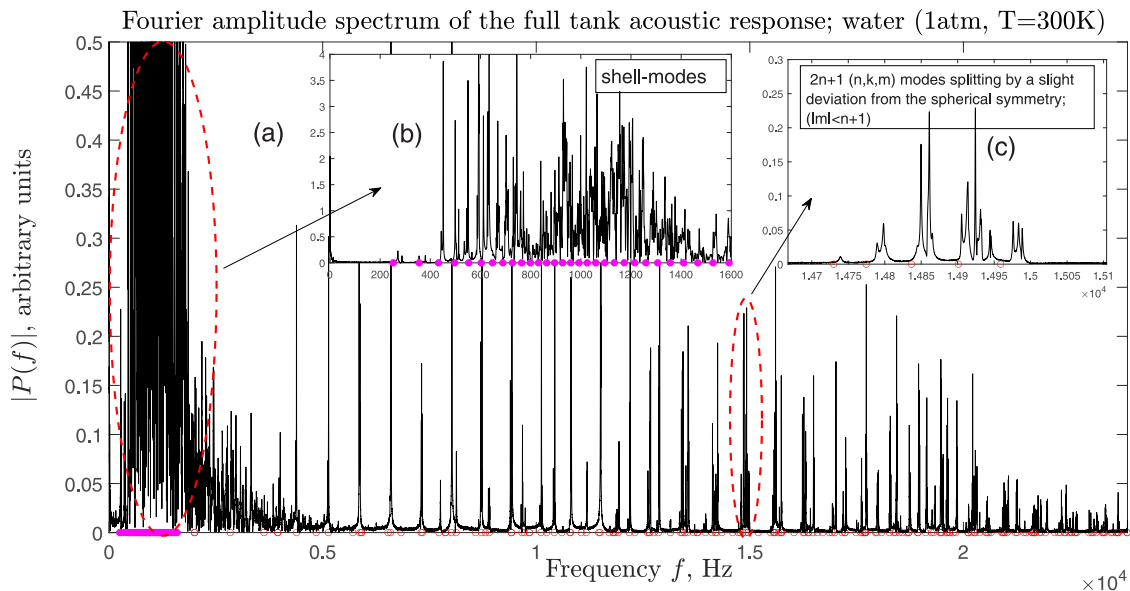

FIG. 5. (Color online) Fourier amplitude spectrum of the acoustic response of the water-filled tank to a single ping of a solenoid actuator (a). Red circles correspond to the liquid modes and magenta dots to the shell modes given by Eq. (15). The dense conglomerate of modes at the lower end of the spectrum, subplot (b), is associated with the shell modes for the azimuthal wave number $n \lesssim 50$, where their density is the highest, as predicted by the theory, see Fig. 3. The predicted shell mode locations at high wavenumbers n are not shown. The splitting of the degenerate modes by a slight deviation of the tank geometry from spherical symmetry is shown in subplot (c).

J. Acoust. Soc. Am. **152** (6), December 2022
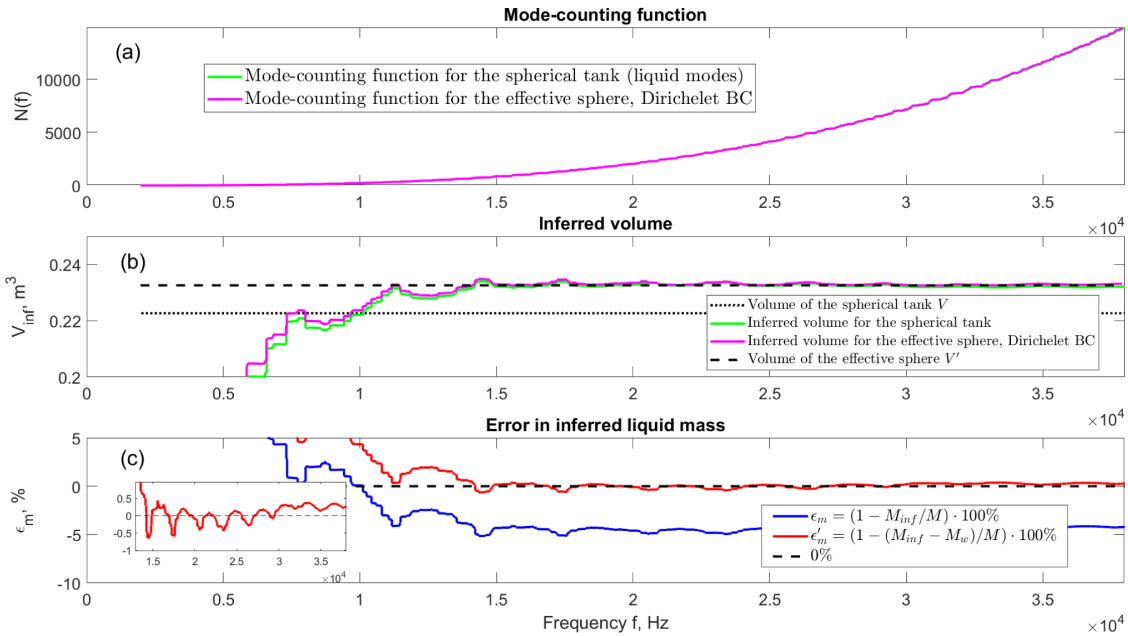
Muratov *et al.* 3265

FIG. 6. (Color online) (a) Liquid-modes counting function $N(f)$, Eq. (15) (green) vs liquid-modes counting function $N'(f)$, corresponding to an effective sphere of radius $R' = R/(1 - \varepsilon)$ and Dirichlet BC (red). (b) The liquid volume inferred from the counting functions $N(f)$ (green) and $N'(f)$ (red), using Richardson's extrapolation to fit the counting functions to Weyl's law, Eq. (4). The dotted and dashed lines designate the tank volume and the volume of the effective sphere, respectively. (c) The error in the mass inference from the counting function $N(f)$ without the wall corrections (blue) and with the wall corrections (red). The insert shows that introducing the wall corrections brings the error into the range of $\pm 0.5\%$ at $f \gtrsim 15$ kHz, corresponding to $N \gtrsim 1000$ modes.

which does not take the added mass into account, $\varepsilon_m = (1 - M_{inf}/M) \cdot 100\%$ and compares it with the error obtained when the added mass of the wall is corrected for, $\varepsilon'_m = (1 - (M_{inf} - M_w)/M) \cdot 100\%$. Here, M_{inf} and M designate the inferred and the actual mass of the liquid, respectively. We see that introducing the wall corrections brings the error into the range of $\pm 0.5\%$ at $f \gtrsim 15$ kHz, corresponding to $N \gtrsim 1000$ modes.

Figure 7 shows the error in the mass inference with and without the wall corrections for a broader range of frequencies extending far beyond the region of validity of the soft-wall approximation, Eq. (19). At $f \gtrsim 40$ kHz, the error of the wall-corrected inference increases with f, while the error of the no-correction inference gradually decreases in the rigid wall limit, $f \gg c_L/(2\pi R \varepsilon)$, as expected.

To summarize, fitting the mode counting function of the spherical tank to Weyl's law overestimates the mass of the liquid by an amount equal to the mass of the tank wall, which can be corrected for when the mass of the wall is known. Although the foregoing calculations pertain to a spherical tank, it can be shown (see Appendix C) that the main result generalizes to thin-walled tanks and liquid configurations of arbitrary shapes. Namely, the liquid modes spectrum of a thin-walled tank is equivalent, in the first order in wall effects, to the spectrum of an infinitesimally thin-walled tank (Dirichlet boundary conditions) of a slightly larger volume, with the added mass equal to the mass of the tank wall in contact with the liquid. This result is independent on the tank shape and liquid configuration. Therefore, Weyl's law for Dirichlet boundary conditions can be applied to infer the mass of the liquid, using the wall

corrections equal to the mass of the wall in contact with the liquid. Under the conditions of microgravity in space the propellant typically wets the tank wall,[26] and the wall correction equals the total mass of the tank wall, which is independent of the liquid configuration and is generally known.

VI. CONCLUSIONS

In conclusion, we carried out a theoretical analysis of the normal modes of a spherical thin-walled water-filled tank. A distinction of shell vs liquid modes was made to facilitate both theoretical and experimental analysis of the spectrum. An experimental validation of the theory for water-filled tank was demonstrated. The correspondence between the experimental data and the theory is excellent. We showed that in the soft wall limit the liquid modes of the tank are identical, in the first order in a certain perturbation parameter, to the spectrum of a sphere with Dirichlet boundary conditions, having a slightly larger volume corresponding to the mass of liquid equal to the mass of liquid in the tank plus the mass of the tank's wall. As a consequence, an application of Weyl's law to infer the mass of the liquid contained in a thin-walled spherical tank from its acoustic response gives an effective mass which is larger than the actual mass of the liquid by the added mass equal to the mass of the wall. This result is generalized to thin-walled tanks and liquid configurations of arbitrary shapes, where the wall corrections are shown to equal the mass of the tank wall in contact with the liquid. This result has important implications for propellant tanks in the microgravity conditions in space, since typically the propellant wets the tank
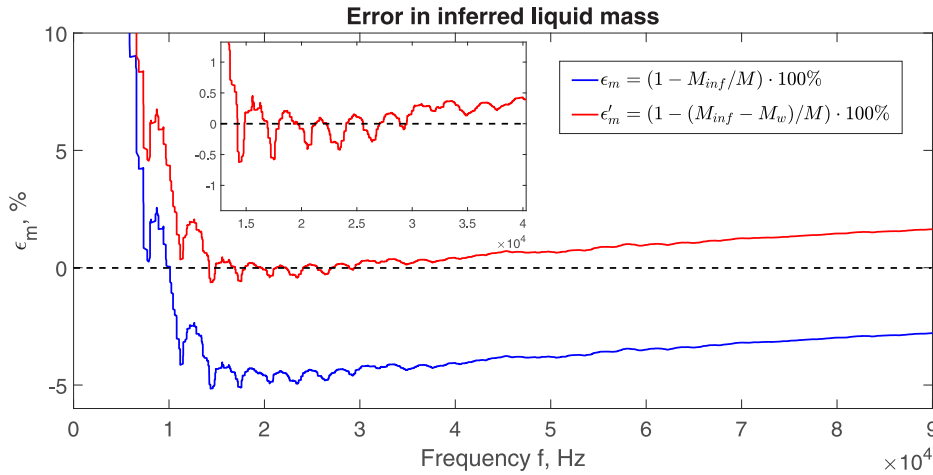
Error in inferred liquid mass

FIG. 7. (Color online) The error in mass inference using Richardson extrapolation from the counting function $N(f)$, without the wall corrections (blue) and with the wall corrections (red). The insert shows that introducing the wall corrections brings the error into the range of $\pm 0.5\%$ at $15\,\mathrm{kHz} \lesssim f \lesssim 40\,\mathrm{kHz}$, corresponding well to the soft wall intermediate asymptotic regime $f \ll c_L/(2\pi R\varepsilon)$ described by Eq. (19). At higher frequencies, $f \gtrsim c_L/(2\pi R\varepsilon)$, the error with wall corrections starts to increase, while the error without the wall correction decreases in absolute value gradually reflecting a transition to the rigid wall limit.

wall, in which case the mass of the wall in contact with the propellant equals the total mass of the wall. Although the propellant configuration under microgravity conditions is generally unknown, the tank wall total mass is known and the wall correction can be readily made to infer the propellant mass based on an application of Weyl's law for Dirichlet boundary conditions to the acoustic spectrum of the tank.

ACKNOWLEDGMENTS

APPENDIX A: ANALYSIS OF THE ROOTS OF THE CHARACTERISTIC EQUATION

Here, we present the details of the argument that shows that there is exactly one root $\lambda_{n,k} \in (a'_{n,k}, a'_{n,k+1})$ of Eq. (15) for every $k = 0, 1, 2, \ldots$, where $a'_{n,k}$ denotes the kth root of $j'_n(z)$, with the convention that $a'_{n,0} = 0$.

Notice that Eq. (15) may be rewritten with the help of Eq. (13) as

$$\varepsilon + \frac{j_n(\lambda)}{\lambda j'_n(\lambda)} = \frac{\kappa_n}{\lambda^2}. \tag{A1}$$

We claim that the left-hand side of Eq. (A1) is a monotonically increasing function of λ for all $\lambda \neq a'_{n,k}$. To prove it, we need to show that

$$-\frac{\lambda j_n^2(\lambda) + \lambda j_{n+1}^2(\lambda) - (2n+1) j_n(\lambda) j_{n+1}(\lambda)}{j_n^2(\lambda)}$$
$$= \frac{d}{d\lambda}\left(\frac{\lambda j'_n(\lambda)}{j_n(\lambda)}\right) \leq 0, \tag{A2}$$

whenever $\lambda \neq a_{n,k}$, where $a_{n,k}$ is the kth root of $j_n(z)$. The equality in Eq. (A2) follows from the differential equation satisfied by $j_n(z)$ [see Eq. (10.1.1) in Ref. 23] and Eq. (13).

Let $r_n(\lambda) = j_{n+1}(\lambda)/j_n(\lambda)$. Then the claim in Eq. (A2) is equivalent to

$$1 + r_n^2(\lambda) - \frac{2n+1}{\lambda} r_n(\lambda) \geq 0. \tag{A3}$$

The latter is clearly true for $\lambda > n + (1/2)$, as can be easily seen by completing the square. Therefore, we now focus on the range of $\lambda \leq n + (1/2)$ and begin by observing that from the recurrence relation in Eq. (10.1.19) of Ref. 23 it follows that Eq. (A3) is equivalent to

$$r_n(\lambda) \leq r_{n-1}(\lambda). \tag{A4}$$

To verify the latter, we appeal to the continued fraction representation of $r_n(z)$ given by Eq. (17.10.40) of Ref. 27,

$$r_n(\lambda) = \cfrac{\lambda}{2n+3 - \cfrac{\lambda}{2n+5 - \cfrac{\lambda}{2n+7 - \cdots}}}. \tag{A5}$$

By inspection, for $\lambda \leq n + (1/2)$ the inequality in Eq. (A4) holds for every convergent of the continued fraction representations of r_n and r_{n-1}. Passing to the limit then yields the claim.

As a corollary to the inequality in Eq. (A4), we can establish an explicit lower bound on the values of $a'_{n,1}$. This result follows from Eqs. (10.1.55)-(10.1.56) in Ref. 23, which in the notation of this appendix read $r_n(a'_{n,1}) = n/a'_{n,1}$ and $r_{n-1}(a'_{n,1}) = a'_{n,1}/(n+1)$. Inserting those expressions into Eq. (A4) yields

$$a'_{n,1} \geq \sqrt{n(n+1)}. \tag{A6}$$

In addition, since there is exactly one root $\lambda_{n,k} \in (a'_{n,k}, a'_{n,k+1})$, the inequality in Eq. (A6) implies that

$$\lambda_{n,k} > \sqrt{n(n+1)}, \quad k > 0. \tag{A7}$$

APPENDIX B: VANISHING ELASTICITY LIMIT

Using Eq. (A7), we can derive a condition under which the elasticity term κ_n/λ^2 in Eq. (15) can be neglected for the calculation of $\lambda_{n,k}$ for $k > 0$. Let $\lambda_{n,k}^{(0)}$ denote the solution of

$$\varepsilon + \left(n - \frac{\lambda j_{n+1}(\lambda)}{j_{n,k}(\lambda)} \right)^{-1} = 0, \tag{B1}$$

and consider the term κ_n/λ^2 in Eq. (15) as a perturbation to Eq. (B1). In the first order in the perturbation we have $\lambda_{n,k} - \lambda_{n,k}^{(0)} = \lambda_{n,k}^{(1)}$, with the first order correction given by

$$\lambda_{n,k}^{(1)} = \frac{\kappa_n}{\left(\lambda_{n,k}^{(0)} \right)^2} \left(\frac{dy}{d\lambda} \right)^{-1} \Bigg|_{\lambda = \lambda_{n,k}^{(0)}}, \tag{B2}$$

where $y(\lambda)$ denotes the left-hand side of Eq. (B1). Since $|\lambda_{n,k+1} - \lambda_{n,k}| \sim |a'_{n,k+1} - a'_{n,k}| \sim 1$, the term κ_n/λ^2 in Eq. (15) can be neglected provided $\lambda_{n,k}^{(1)} \ll 1$, or

$$\frac{\kappa_n}{\left(\lambda_{n,k}^{(0)} \right)^2} \ll \left(\frac{dy}{d\lambda} \right) \Bigg|_{\lambda = \lambda_{n,k}^{(0)}}. \tag{B3}$$

The differentiation of the left-hand side of Eq. (B1) may be performed using Eqs. (10.1.21) and (10.1.22) in Ref. 23 to express the result as a function of $r_n(\lambda) = j_{n+1}(\lambda)/j_n(\lambda)$. Noting that $r_n(\lambda_{n,k}^{(0)}) = [n + (1/\varepsilon)]/\lambda_{n,k}^{(0)}$ by Eq. (B1), we obtain that Eq. (B3) is equivalent to

$$\frac{\kappa_n}{\left(\lambda_{n,k}^{(0)} \right)^2} \ll \frac{1 - \varepsilon + \varepsilon^2 \left[(\lambda_{n,k}^{(0)})^2 - n(n+1) \right]}{\lambda_{n,k}^{(0)}}. \tag{B4}$$

Finally, we use Eq. (A7) to derive a stronger smallness condition

$$\kappa_n \ll (1 - \varepsilon) \sqrt{n(n+1)}. \tag{B5}$$

If Eq. (B5) is satisfied, then so is Eq. (B4), and it can be expected that the elasticity term κ_n/λ^2 introduces small corrections to the roots of Eq. (15) and can be neglected in the leading order of the perturbation theory.

We now focus on the limiting regimes for solutions of Eq. (B1). In the limit $\lambda \ll \varepsilon^{-1}$, we look for the solution in the form $\lambda_{n,k} = a_{n,k} + \lambda_{n,k}^{(1)}$, where $a_{n,k}$ is the kth zero of $j_n(z)$. Using the equivalent form

$$\varepsilon + \frac{j_n(\lambda)}{\lambda j'_n(\lambda)} = 0 \tag{B6}$$

of Eq. (B1) with the above ansatz for $\lambda_{n,k}$ and linearizing the resulting equation in $\lambda_{n,k}^{(1)}$ gives $\lambda_{n,k}^{(1)} = -\varepsilon a_{n,k}$, i.e.,

$$\lambda_{n,k} \simeq a_{n,k}(1 - \varepsilon), \quad \lambda_{n,k} \ll \varepsilon^{-1}. \tag{B7}$$

For Eq. (B7) to be self-consistent, the first order correction term $a_{n,k}\varepsilon$ has to be much smaller than the spacing between the subsequent zeros $a_{n,k}$, i.e., $a_{n,k}\varepsilon \ll |a_{n,k} - a_{n,k\pm1}| \sim 1$. Thus, we confirm the validity condition $a_{n,k}\varepsilon \ll 1$ for the approximation in Eq. (B7), which resolves an apparent contradiction between the shrinkage of the distance between the subsequent roots $\lambda_{n,k}$ and $\lambda_{n,k+1}$ by the factor $(1 - \varepsilon)$

compared to the unperturbed roots $a_{n,k}$ and $a_{n,k+1}$, and the fact that all roots $\lambda_{n,k}$ are sandwiched between the zeros $a'_{n,k}$ and $a'_{n,k+1}$ as proved in Appendix A.

In the opposite limit $\lambda \gg \varepsilon^{-1}$, we look for solution in the form $\lambda_{n,k} = a'_{n,k} + \lambda_{n,k}^{(1)}$, where $a'_{n,k}$ is the kth zero of $j'_n(z)$. We first rewrite Eq. (B6) in the form

$$\frac{j'_n(\lambda)}{j_n(\lambda)} = -(\lambda\varepsilon)^{-1}. \tag{B8}$$

In the leading order of $(\lambda\varepsilon)^{-1} \ll 1$, Eq. (B8) yields

$$\lambda_{n,k}^{(1)} = -\frac{j_n(a'_{n,k})}{\varepsilon a'_{n,k} j''_n(a'_{n,k})}. \tag{B9}$$

Using the differential equation satisfied by $j_n(z)$ [see Eq. (10.1.1) in Ref. 23] and the property $j'_n(a'_{n,k}) = 0$, we have

$$j''_n(a'_{n,k}) = -j_n(a'_{n,k}) \left(1 - \frac{n(n+1)}{(a'_{n,k})^2} \right), \tag{B10}$$

which yields

$$\lambda_{n,k}^{(1)} = \frac{1}{\varepsilon a'_{n,k} \left(1 - \frac{n(n+1)}{(a'_{n,k})^2} \right)}. \tag{B11}$$

Notice that by Eq. (A6) we have $\lambda_{n,k}^{(1)} > 0$ for all $k \geq 1$. Once again, the validity condition for Eq. (B11) is $\lambda_{n,k}^{(1)} \ll |a'_{n,k+1} - a'_{n,k}| \sim 1$. Using Eq. (B11), it can be expressed as follows:

$$\lambda_{n,k} \gg (2\varepsilon)^{-1} + \sqrt{(2\varepsilon)^{-2} + n(n+1)}. \tag{B12}$$

We see that condition $\lambda_{n,k} \gg \varepsilon^{-1}$ is a necessary but not a sufficient condition for the rigid wall (Neumann boundary conditions) approximation. We note that in contrast to the soft-wall limit $\lambda_{n,k}\varepsilon \ll 1$, in which all modes in the frequency range are approximated well by those corresponding to the Dirichelet boundary condition, the rigid wall approximation breaks down for modes where $\lambda_{n,k} \sim n$.

Putting everything together, in the rigid wall limit we obtain

$$\lambda_{n,k} \simeq a'_{n,k} + \frac{1}{\varepsilon a'_{n,k} \left(1 - \frac{n(n+1)}{(a'_{n,k})^2} \right)}, \tag{B13}$$

$$\lambda_{n,k} \gg (2\varepsilon)^{-1} + \sqrt{(2\varepsilon)^{-2} + n(n+1)}.$$

APPENDIX C: WALL CORRECTIONS. GENERAL CASE

Here, we consider a thin-walled tank and a liquid configuration of arbitrary shape, where the liquid is in contact with the wall all over its surface. Such liquid configurations are expected to form under microgravity conditions in

space, where the propellant wets the tank wall. To compute the tank-wall correction, we use a first-order perturbation theory in the shell effect. As we saw in Sec. III, the liquid modes are described by Eq. (18), corresponding to the boundary conditions in Eq. (10), where the B and S terms are taken to be zero. In this approximation, the boundary condition in Eq. (10) becomes

$$\rho_w d_w \partial_t^2 \zeta = -\rho_L \partial_t \varphi \quad \text{on} \quad \partial B. \tag{C1}$$

Using Eq. (6), we can then shape the boundary conditions Eq. (C1) into the following Robin boundary condition:

$$\frac{\rho_w d_w}{\rho_L} \partial_n \varphi + \varphi = 0 \quad \text{on} \quad \partial B. \tag{C2}$$

We are interested in the soft wall limit, when $\rho_w d_w k / \rho_L \ll 1$, where k is the magnitude of the wavevector corresponding to the liquid mode. In this limit, the spectrum is a perturbation to the spectrum associated with the Dirichlet boundary condition. The physical interpretation of the condition above is that the mass of the liquid contained in the liquid layer of the wavelength width is much larger than the weight of the wall per unit area. Using Eq. (9.2.25) from Ref. 28, we obtain the following characteristic equation for the spectrum of the Laplacian operator with the Robin boundary condition, corresponding to a weak perturbation of the Dirichlet boundary condition as in Eq. (C2):

$$\left| (k^2 - k_p^2)\delta_{pq} + \frac{\rho_w d_w}{\rho_L} \frac{k^2}{k_p k_q} \int_{\partial B} \partial_n \bar{\phi}_p \partial_n \phi_q ds \right| = 0, \tag{C3}$$

where ϕ_q are the unperturbed Dirichlet eigenfunctions, bar stands for complex conjugate and the integration is performed over the tank wall in contact with the liquid. We note that for wetting propellants in space the integration runs over the entire wall. In the first order of the perturbation theory, only the diagonal terms in the perturbation matrix in Eq. (C3) should be considered, which leads to

$$k_p^2 = (k_p^{(0)})^2 - \frac{\rho_w d_w}{\rho_L} \int_{\partial B} |\partial_n \phi_p|^2 ds, \tag{C4}$$

corresponding to Eq. (19) above for the sphere.

Next, we consider a different perturbation theory, where the boundaries of an infinitely thin-walled tank are perturbed in such a way that the perturbed boundary corresponds to ∂B and the unperturbed boundary to $\partial B'$. Since the walls are infinitesimally thin, the Dirichlet boundary conditions are taken. Using Eqs. (9.2.71), (9.2.49), and (9.2.51) from Ref. 28, we obtain the following expression for the first-order perturbation of the liquid spectrum for the full tank:

$$k_p^2 - (k_p^{(0)})^2 + \int_{\partial B} (\partial_n \overline{\phi'}_p) \phi'_p ds = 0, \tag{C5}$$

where ϕ'_q are the unperturbed Dirichlet eigenfunctions, corresponding to the original boundary $\partial B'$, and the integration

is performed over the perturbed boundary ∂B. In the first order in the perturbation of the boundary, we can write $\phi'_p = -(\partial_n \phi'_p)|_{\partial B'} \delta r$, where δr is the local distance between $\partial B'$ and ∂B. In addition, in the first order of the perturbation theory for the eigenvalues we can take $(\partial_n \phi'_p)|_{\partial B'} = (\partial_n \phi'_p)|_{\partial B} = \partial_n \phi_p|_{\partial B}$ in the integral in Eq. (C5). This brings Eq. (C5) to the form

$$k_p^2 - (k_p^{(0)})^2 - \int_{\partial B} |\partial_n \phi_p|^2 \delta r ds = 0. \tag{C6}$$

We consider the following specific perturbation of the boundary: $\delta r = \rho_w d_w / \rho_L$. Using this perturbation, we can cast Eq. (C6) into the following form:

$$(k_p^{(0)})^2 = k_p^2 - \frac{\rho_w d_w}{\rho_L} \int_{\partial B} |\partial_n \phi_p|^2 ds, \tag{C7}$$

where $(k_p^{(0)})^2$ is the liquid spectrum of the full infinitesimally thin-walled tank (i.e., with the Dirichlet boundary condition) with the boundary $\partial B'$ and k_p^2 is the spectrum of the infinitely thin-walled tank with the boundary ∂B. Therefore, k_p^2 in Eq. (C7) equals $(k_p^{(0)})^2$ in Eq. (C4). It follows that $(k_p^{(0)})^2$ in Eq. (C7) equals k_p^2 in Eq. (C4). Accordingly, we obtain the following interpretation of the perturbed spectrum k_p^2 in Eq. (C4): this spectrum is identical (in the first order in the shell effect) to the unperturbed spectrum of the full infinitely thin-walled tank (i.e., with the Dirichlet boundary condition) with a boundary $\partial B'$, such that $\delta r = \rho_w d_w / \rho_L$. The effective mass of the liquid contained inside the boundary $\partial B'$ is larger than the mass of the liquid contained inside the boundary $\partial B'$ by the amount

$$\delta M = \rho_L \int_{\partial B} \delta r ds = \rho_L \int_{\partial B} \frac{\rho_w d_w}{\rho_L} ds = \rho_w d_w \int_{\partial B} ds = M_w, \tag{C8}$$

i.e., by the mass of the wall.

[1]M. L. Meyer, D. J. Chato, D. W. Plachta, G. A. Zimmerli, S. J. Barsi, N. T. Van Dresar, and J. P. Moder, "Mastering cryogenic propellants," J. Aerosp. Eng. **26**, 343–351 (2013).

[2]D. Miranda, NASA Technology Taxonomy, NASA Report No. HQ-E-DAA-TN76545 (2020).

[3]B. Yendler, "Review of propellant gauging methods," in *AIAA Aerospace Sciences Meeting and Exhibit* (2006).

[4]F. T. Dodge, "Propellant mass gauging: Database of vehicle applications and research and development studies," NASA Technical Report No. CR-2008-215281 (2008).

[5]J. Parson, K. Roe, J. Feller, M. Khasin, and S. P. Sharma, "Mass gauging for sustained presence in outer space: A technology review," in *AIAA Scitech 2021 Forum* (2021).

[6]A. J. Mord, H. A. Snyder, K. A. Kilpatrick, L. A. Hermanson, R. A. Hopkins, and D. A. Vangundy, Fluid Quantity Gaging, Contractor Report No. NASA-CR-185516 (1988).

[7]R. S. Roberts, J. T. Chen, O. A. Vela, and P. S. Lewis, "Munitions classification using an acoustic resonance spectroscopic technique," in *Proceedings of 27th Asilomar Conference on Signals, Systems and Computers* (1993), Vol. **2**, pp. 991–995.

[8]K. M. Crosby, T. Rundle, K. LeCaptain, and R. Werlink, "Modal propellant gauging in low gravity," in *AIAA Space 2016* (2016), p. 5533.

J. Acoust. Soc. Am. **152** (6), December 2022

Muratov *et al.* 3269

[9]J. R. Feller, A. Kashani, M. Khasin, C. B. Muratov, V. V. Osipov, and S. Sharma, Spectral mass gauging of unsettled liquid with acoustic waves. NASA Technical Report No. TM–2018–219876 (2018).

[10]G. A. Zimmerli, M. Asipauskas, C. M. Dong, R. P. Wade, S. L. Metzger, and A. M. O'Connor, "Radio frequency mass gauge (RFMG) test results from Robotic Refueling Mission 3 (RRM3) operations on International Space Station (ISS)," Technical Report No. NASA/TP-20205000671 (2020).

[11]H. Weyl, "Über die asymptotische Verteilung der Eigenwerte," ("About the asymptotic distribution of the eigenvalues"), Nachrichten von der Gesellschaft der Wissenschaften zu Göttingen, Mathematisch-Physikalische Klasse (1911), pp. 110–117.

[12]W. Arendt, R. Nittka, W. Peter, and F. Steiner, " 'Weyl's law: Spectral properties of the Laplacian in mathematics and physics," in *Mathematical Analysis of Evolution, Information, and Complexity*, edited by W. Arendt and W. P. Schleich (Wiley-VCH, Weinheim, 2009).

[13]R. H. Bolt, "Frequency distribution of eigentones in a three-dimensional continuum," J. Acoust. Soc. Am. **10**, 228–234 (1939).

[14]D. Y. Maa, "Distribution of eigentones in a rectangular chamber at low frequency range," J. Acoust. Soc. Am. **10**, 235–238 (1939).

[15]R. H. Bolt, "Normal frequency spacing statistics," J. Acoust. Soc. Am. **19**, 79–90 (1947).

[16]K. A. Gillis, J. B. Mehl, J. W. Schmidt, and M. R. Moldover, " 'Weighing' a gas with microwave and acoustic resonances," Metrologia **52**, 337–352 (2015).

[17]M. R. Moldover, J. B. Mehl, and M. Greenspan, "Gas-filled spherical resonators: Theory and experiment," J. Acoust. Soc. Am. **79**(2), 253–272 (1986).

[18]C. Guianvarc'h and L. Pitre, "Acoustic field in a quasi-spherical resonator: Unified perturbation model," J. Acoust. Soc. Am. **125**, 1416–1425 (2009).

[19]J. B. Lonzaga, J. L. Raymond, and J. Mobley, "Suppression of an acoustic mode by an elastic mode of a liquid-filled spherical shell resonator," J. Acoust. Soc. Am. **129**, 597–603 (2011).

[20]L. D. Landau and E. M. Lifshitz, *Course of Theoretical Physics* (Pergamon Press, London, 1987), Vol. 6.

[21]E. Reissner, "Stresses and small displacements of shallow spherical shells. I," J. Math. Phys. (Cambridge, Mass.) **25**, 80–85 (1946).

[22]A. Vaziri and L. Mahadevan, "Localized and extended deformations of elastic shells," Proc. Natl. Acad. Sci. U.S.A. **105**, 7913–7918 (2008).

[23]M. Abramowitz and I. Stegun, *Handbook of Mathematical Functions* (National Bureau of Standards, Washington, DC, 1964).

[24]L. Delzeit, J. Feller, B. Helvensteijn, A. Kashani, M. Khasin, and V. Osipov, "Spectral mass gauging of liquids with acoustic waves," in *50th International Conference on Environmental Systems*, paper No. ICES-2021-293 (2021), pp. 12–15.

[25]L. F. Richardson, "The approximate arithmetical solution by finite differences of physical problems including differential equations, with an application to the stresses in a masonry dam," Philos. Trans. R. Soc. A **210**, 307–357 (1911).

[26]J. W. Hartwig, *Liquid Acquisition Devices for Advanced in-Space Cryogenic Propulsion Systems* (Elsevier, New York, 2016).

[27]A. Cuyt, V. B. Petersen, B. Verdonk, H. Waadeland, and W. B. Jones, *Handbook of Continued Fractions for Special Functions* (Springer, New York, 2008).

[28]P. M. Morse and H. Feshbach, *Methods of Theoretical Physics* (McGraw-Hill, New York, 1953), Vol. 2.

3270   J. Acoust. Soc. Am. **152** (6), December 2022

Muratov *et al.*